Chirp effect in hard X-ray generation from liquid target when irradiated by femtosecond pulses

doi: 10.1364/OE.16.012650

Chirp effect in hard X-ray generation from liquid target when irradiated by femtosecond pulses

Koji Hatanaka[1], Takahito Ida[2], Hiroshi Ono[2], Shin-ichi Matsushima[2], Hiroshi Fukumura [2], Saulius Juodkazis [3], and Hiroaki [3]Misawa

[1] *Center for Ultrafast Intense Laser Science, Graduate School of Science, The University of Tokyo, Tokyo 113-0033, Japan*

[2] *Department of Chemistry, Graduate School of Science, Tohoku University, Sendai 980-8578, Japan*

[3] *Research Institute for Electronic Science, Hokkaido University, CRIS Bldg., Sapporo 001-0021, Japan*

hatanaka@chem.s.u-tokyo.ac.jp; fukumura@mail.tains.chem. tohoku.ac.jp

Abstract: The chirp effect on a X-ray emission intensity from a CsCl aqueous solution jet irradiated by femtosecond pulses was systematically studied. The *p*-polarized chirped pulses were more efficient as compared with the shortest pulses determined by the spectral bandwidth. The negatively-chirped pulses of approximately 240 fs duration produced up to 10 times larger X-ray intensity as compared with the transform-limited 160 fs pulses. The angular dependence of X-ray generation can be explained by the resonant absorption. Numerical simulations of electron density evolution due to the avalanche and multi-photon absorption supports qualitatively well the experimental observations.

OCIS codes: (320.1590) Chirping; (340.7480) X-rays, soft x-rays, extreme ultraviolet (EUV); (350.5400) Plasmas; (190.4180) Multiphoton processes.

References and links

1. M. M. Murnane, C. Kapteyn, M. D. Rosen, and R. W. Falcone, "Ultrafast X-ray pulses from laser-produced plasmas," Science **251**, 531 – 536, (1991).
2. J. Workman, M. Nantel, A. Maksimchuk, and D. Umstadler, "Application of a picosecond soft x-ray source to time-resolved plasma dynamics," Appl. Phys. Lett. **70**, pp. 312– 314, (1997).
3. D. F. Price, R. M. More, R. S. Walling, G. Guethlein, R. L. Shepherd, R. E. Stewart, and W. E. White, "Absorption of ultrashort laser pulses by solid targets heated rapidly to temperatures 1-1000 eV," Phys. Rev. Lett. **75**, 252 – 255, (1995).
4. C. W. Siders, A. Cavalleri, K. Sokolowski-Tinten, C. Toth, T. Guo, M. Kammler, M. H. von Hoegen, K. R. Wilson, D. von der Linde, and C. P. J. Barty, Science **286**, 1340, (1999).
5. P. Audebert, P. Renaudin, S. Bastiani-Ceccotti, J.-P. Geindre, C. Chenais-Popovics, S. Tzortzakis, V. Nagels-Silvert, R. Shepherd, I. Matsushima, S. Gary, F. Girard, O. Peyrusse, , and J.-C. Gauthier, "Picosecond time-resolved X-Ray absorption spectroscopy of ultrafast aluminum plasmas," Phys. Rev. Lett. **94**, 025004/1–4, (2005).
6. J.-C. Gauthier, J.-P. Geindre, P. Audebert, and A. R., "Observation of KL - LL x-ray satellites of aluminum in femtosecond laser-produced plasmas," Phys. Rev. E **52**, 2963 – 2968, (1995).
7. C. Bressler and M. Chergui, "Ultrafast x-ray absorption spectroscopy," Chem. Rev. **104**, 1781 – 1812, (2004).
8. D. Mathur, "Structure and dynamics of molecules in high charge states," Phys. Rep. **391**(1-2), 1 – 118, (2004).
9. H. Nakano, T. Nishikawa, and N. Uesugi, "Soft x-ray pulse generation from femtosecond laser-produced plasma with reduced debris using a metal-doped glass target," Appl. Phys. Lett. **70**, 16–18, (1997).

#96969 - $15.00 USD Received 4 Jun 2008; revised 17 Jul 2008; accepted 29 Jul 2008; published 6 Aug 2008

10. C. Y. Cô té , J. C. Kieffer, Z. Jiang, A. Ikhlef, and H. Pépin J. Phys. B: At. Mol. Opt. Phys. **31**, L883–L889, (1998).
11. M. Anand, C. P. Safvan, and M. Krishnamurthy, "Hard X-ray generation from microdroplets in intense laser fields," Appl. Phys. B **81**, 469–477, (2005).
12. G. Korn, A. Thoss, H. Stiel, U. Vogt, M. Richardson, and T. Elsaesser, "Ultrashort 1-khz laser plasma hard x-ray source," Opt. Lett. **27**, 866 – 868, (2002).
13. K. Hatanaka, T. Miura, and H. Fukumura, "White X-ray pulse emission of alkali halide aqueous solutions irradiated by focused femtosecond laser pulses: a spectroscopic study on electron temperatures as function of laser intensity, solute concentration, and solute atomic number," Chem. Phys. **299**, 265–270, (2004).
14. K. Hatanaka, T. Miura, and H. Fukumura, "Ultrafast X-ray pulse generation by focusing femtosecond infrared laser pulses onto aqueous solutions of alkali metal chloride," Appl. Phys. Lett. **80**, 3925–3927, (2002).
15. M. Silies, S. Linden, H. Witte, and H. Zacharias, "The dependence of the Fe K_α yield on the chirp of the femtosecond exciting laser pulse," Appl. Phys. B **87**, 623 – 627, (2007).
16. H. Misawa and S. Juodkazis, *3D laser microfabrication: principles and applications*, (Weinheim, Wiley-VCH, 2006) ch. 9.
17. S. Juodkazis, K. Nishimura, and H. Misawa, "Three-dimensional laser structuring of materials at tight focusing," Chin. Opt. Lett. **5**, S198 – 200, (2007).
18. D. Attwood, *Soft X-rays and extreme ultraviolet radiation: principles and applications*, (Cambridge, Cambridge University Press, 1999).
19. N. I. Koroteev and I. L. Shumai, *Physics of high-intensity laser radiation*, (Moscow, Nauka (in Russ.), 1991).
20. F. Brunel, "Not-so-resonant, resonant absorption," Phys. Rev. Lett. **59**, 52 – 55, (1987).
21. A. V. Getz and V. P. Krainov, "Vacuum heating of large atomic clusters by superintense femtosecond laser pulse," J. Exper. & Theor. Phys. **101**, 80–87, (2005).
22. V. I. Berezhiani, S. M. Mahajan, Z. Yoshida, and M. Pekker, "Dynamics of self-trapped singular beams in an underdense plasma," Phys. Rev. E **65**, 046415, (2002).
23. A. Vogel, J. Noack, G. Hüttman, and G. Paltauf, "Mechanisms of femtosecond laser nanosurgery of cells and tissues," Appl. Phys. B **81**, 1015–1047, (2005).
24. N. Vogel and V. Skvortsov, "The x-ray emission from vacuum discharge micro fragments at comparatevly low applied voltages," IEEE Trans. Plasma Sci. **27**, 122 – 123, (1999).
25. E. E. Gamaly, S. Juodkazis, K. Nishimura, H. Misawa, B. Luther-Davies, L. Hallo, P. Nicolai, and V. Tikhonchuk, "Laser-matter interaction in a bulk of a transparent solid: confined micro-explosion and void formation," Phys. Rev. B **73**, 214101, (2006).
26. S. Juodkazis, A. V. Rode, E. G. Gamaly, S. Matsuo, and H. Misawa, "Recording and reading of three-dimensional optical memory in glasses," Appl. Phys. B **77**, 361–368, (2003).
27. E. G. Gamaly, A. V. Rode, B. Luther-Davies, and V. T. Tikhonchuk, "Ablation of solids by femtosecond lasers: Ablation mechanism and ablation thresholds for metals and dielectrics," Phys. Plasmas **9**, 949 – 957, (2002).
28. R. J. Goldston and P. Rutherford, *Introduction to Plasma Physics* (London, Inst. of Phys. Publishing, Bristol & Philadelphia, 1997).
29. S. Juodkazis, V. Mizeikis, and H. Misawa, "Three-dimensional structuring of resists and resins by direct laser writing and holographic recording," Adv. Polym. Sci. doi: 10.1007/12–2007–122 (2007), published on line Oct. 27).

1. Introduction

Generation of X-rays by femtosecond pulses can become effective and practical with appearance of table-top lasers with high average power > 10 W at high repetition rate > 10 kHz with applications ranging from X-ray lithography to imaging, monitoring of ultra-fast ionic dynamics, etc. [1–8]. Creation of high plasma densities ($> 10^{22}$ cm^{-3}) and temperatures (> 1 keV) is required for efficient X-ray sources. Selection of the characteristic emission lines of elements can be used for monochromatic X-ray light sources of nanometer wavelengths' for future lithography. Hard-X-rays are also prospective for bio-medical applications since the same quality X-ray images can be obtained by a much shorter exposure of living cells when ultra-short pulses of high brilliance are utilized causing a smaller cumulative exposure dose.

When surfaces of solid targets are irradiated at high irradiance of TW-to-PW/cm^2 typically used in X-ray generation the ablation and debris formation occurs [9]. The liquid jets of metals (e.g., Ga) or water solutions doped with metal ions are prospective candidates for realization of practical hard X-ray sources where the exposed region is refreshed before irradiation [10–14].

Here, we demonstrate the dependence of X-ray emission on chirp of fs-pulses at $s-$ and

#96969 - $15.00 USD Received 4 Jun 2008; revised 17 Jul 2008; accepted 29 Jul 2008; published 6 Aug 2008

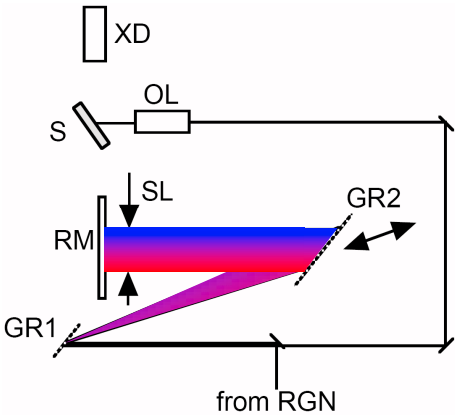

Fig. 1. (color online/final size) Setup used to chirp fs-pulses: XD is the X-ray detector, OL - objective lens, GR1,2 - gratings, S - sample, RM - retro-mirror, SL - slit defining the spectral width, and RNG - regenerative amplifier of fs-pulses. The incoming and outgoing pulses are separated by a slight off-plane angle of mirror (RM).

$p-$polarizations. A systematic study was carried out by measuring X-ray generation using pulses of the same duration with and without positive or negative chirp at the same pulse energy. The pulse duration was independently measured by frequency resolved optical gating (FROG). It is shown that chirp effect can enhance the hard X-ray emission by more than a magnitude, a considerably larger effect than that observed for shorter pulses [15].

2. Experimental

The experimental setup on hard X-ray generation by femtosecond pulses is described in details elsewhere [16]. It consists of femtosecond amplified laser system (CPA2001, Clark MXR with Positive Light Evolution X) delivering 160 fs pulses at 780 nm wavelength with pulse energy up to 1 mJ, focusing optics, a liquid jet sample, and X-ray detector. The fs-pulses were focused on the target, a jet of aqueous solution of CsCl (at 4 mol/dm^3 concentration) using a lens of numerical aperture $NA = 0.28$ (focusing cone angle is 32° in air). The angle of incidence onto the jet was changed from 0° to 90° and the flow rate of solution was 4 mm/ms ensuring complete refresh of the irradiation spot at 1 kHz laser repetition rate. A Geiger-Mueller counter was set at an angle to avoid a specular reflection and to monitor the X-ray emission at 5-10 cm out of the irradiation spot.

Chirp of fs-pulses was controlled by an auxiliary compressor (Fig. 1). The fs-laser output pulses were set to a spectral bandwidth limited length and introduced into the auxiliary compressor comprised of two 1800-lines/mm gratings and a mirror. The chirp was introduced by changing the distance between two parallel gratings (no spatial chirp was introduced [17]).

The length of compressor defines the second order dispersion, the strongest effect in the chirp control. The compressor position for the shortest pulse corresponded to the chirp-free or Fourier transform limited bandwidth pulses with the chirp parameter $\beta = 0$ fs^{-2}; the precision of pre-chirping was approximately 5×10^{-6} fs^{-2}. The pulses were measured by FROG (Swamp Optics, GRENOUILLE) and second harmonic auto-correlation. The pulse duration (at FWHM) was determined using a FROG algorithm numerical retrieval. The slit was set to symmetrically limit the spectrum around the central frequency and to obtain chirp-free pulses of the same duration as the chirped fs-pulses (Fig. 1). This allowed to separate the pulse duration and chirp

#96969 - $15.00 USD Received 4 Jun 2008; revised 17 Jul 2008; accepted 29 Jul 2008; published 6 Aug 2008

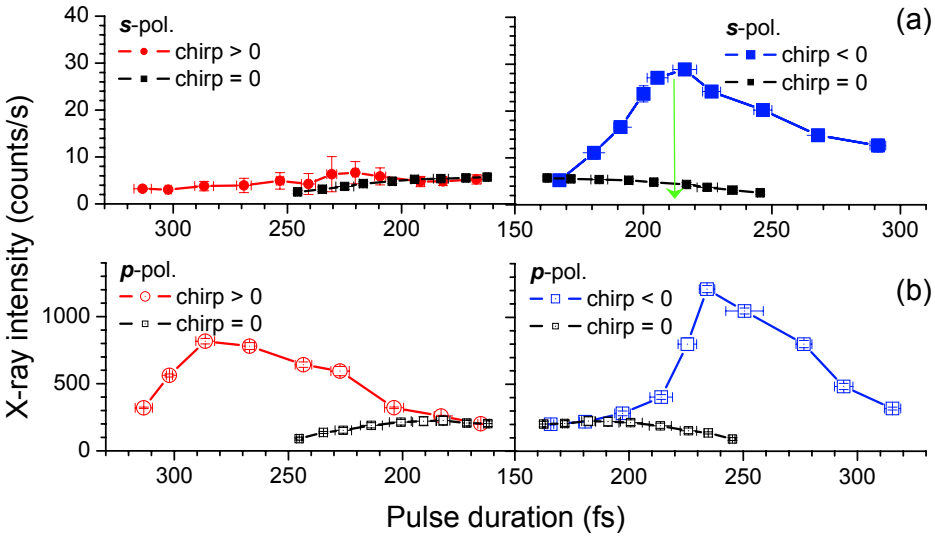

Fig. 2. (color online/final size) The dependence of X-ray intensity on the pulse duration at different values of chirp for $s-$pol. (a) and $p-$pol. (b) in aqueous solution of CsCl (please, note the shortest pulse is at the center of the figure). Pulse energy was $E_p = 0.38$ mJ at focus; the pulse duration was measured before the objective lens. Angle of incidence was 58 degrees. For comparison, X-ray emission by non-chirped transform-limited pulses (controlled by slit SL (Fig. 1)) is also plotted. Arrow (a) marks the shortest pulse duration at the focus.

effects when pulses of the same energy were used in X-ray generation.

3. Results and discussion

Figure 2 summarizes experimental data on the intensity of X-ray at different pulse durations obtained by pre-chirping of 160 fs pulses. There was low efficiency of X-ray generation for $s-$pol. and chirp-free pulses obtained by limiting of spectral width by the slit (Fig. 1). The small increase of X-ray generation for s-pol. was observed for the negative pre-chirp which corresponded to the shortest pulses at the irradiation spot due to the dispersion in the lens (marked by arrow in Fig. 2(a)). As expected, the $p-$pol. with component of incident electric field perpendicular to the target's surface enhances approximately tenfold the X-ray emission at the optimized chirp. This is a considerably larger enhancement as observed from Fe targets [15]. The enhancement was observed for the positive and negative chirp (Fig. 2(b)). The highest emission of hard X-rays was observed at negative chirp when pulse duration was approximately 240 ± 10 fs. The origin of the chirp effect is discussed below together with results of numerical simulations.

The pulses with optimized negative chirp were then used to irradiate target at different incident angles (Fig. 3). The strongest X-ray emission was observed at the angle $\theta = 58^\circ \pm 10^\circ$. The Fresnel reflection $R_p = 0$ would be expected at the Brewster angle of $\theta_B = 54^\circ$ for irradiation of water solution. Due to low refractive index contrast between solution and air the Fresnel reflection is small and cannot account alone for the strong angular dependence in X-ray emission observed experimentally. The resonant absorption [18] can explain the observation as discussed below.

At large incidence angles of the focused laser pulses, the resonant absorption becomes im-

#96969 - $15.00 USD Received 4 Jun 2008; revised 17 Jul 2008; accepted 29 Jul 2008; published 6 Aug 2008

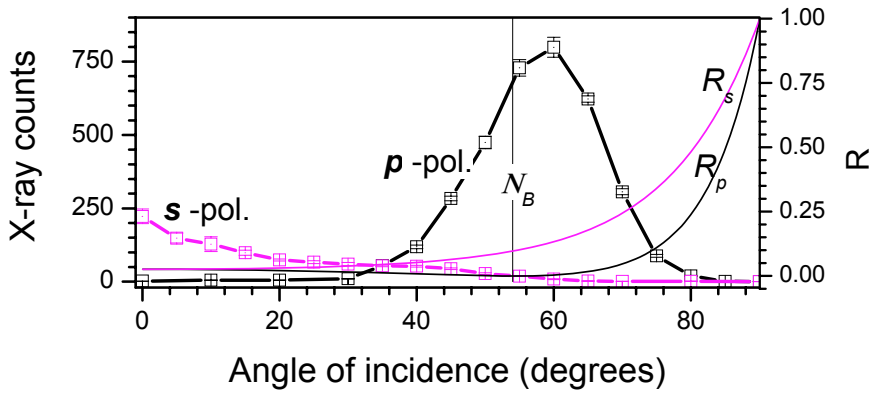

Fig. 3. (color online/final size) Laser incident angle dependence of the X-ray emission from the CsCl aqueous solution (4 mol/dm^3) for $s-$ and $p-$pol. Superimposed are the Fresnel reflection coefficients $R_{p,s}$ (left axis) for the corresponding polarizations at the air-CsCl aqueous solution interface (the refractive indices are $n_{air} = 1$, $n_{sol.} = 1.38$; the Brewster angle $\theta_B = 54^\circ$). Pulse energy was 0.30 mJ; X-ray detector was at 10 cm distance for the p-pol. and at 5 cm for s-pol.

portant. The resonance absorption [18], the main mechanism for plasma heating in the case of nanosecond pulses, depends on focusing and the depth position of the plasma region with critical density where the most efficient absorption takes place. The theoretical limit of irradiance achievable via the resonance absorption is $0.5I_i$. The effective absorption of the incident irradiation, I_i, at the oblique angle of incidence, θ, is given [19]:

$$\frac{I_i - I_r}{I_i} = \frac{\tau(\theta)}{2}\left(2.31\exp(-2\tau(\theta)^3/3)\right)^2, \tag{1}$$

where I_r is the reflected intensity with $\tau(\theta) = \sqrt[3]{\omega z_c/c} \times \sin\theta$ where z_c is the depth position (axial) of the critical plasma density, c and ω are the speed of light and cyclic frequency, respectively.

The eqn. 1 implies that there is an optimum angle of incidence for the most efficient plasma heating by resonant absorption: $\sin(\theta_{opt}) \simeq 0.8\sqrt[3]{c/\omega z_c}$ with the angular width of $\Delta\theta_{opt} \propto \sqrt[3]{c/\omega z_c}$ [18, 19]. One would find that the $\theta_{opt} \simeq 58^\circ$ with $\Delta\theta_{opt} \simeq 49^\circ$ for $z_c \simeq 0.2$ μm at $\lambda \simeq 0.8$ μm wavelength (θ_{opt} and $\Delta\theta_{opt}$ decreases for larger z_c). This would correspond to the plasma emission from a pre-surface layer comparable with the skin depth of a fully ionized water and explains qualitatively well the experimental observation. Due to the focusing cone of 32° ($NA = 0.28$) the experimental angular dependence (Fig. 3) is a convolution and explains broad peak centered around the 58°. It is noteworthy, that more shallow location of critical plasma ($z_c \to 0$), when Brunel mechanism could play an important role, would correspond to $\theta_{opt} \to \pi/2$. Hence, the resonance absorption is not compatible which the Brunel mechanism (also, called a vacuum heating) for which a distinct material-air boundary is necessary [20–22]. Since the Brunel mechanism is not angularly dependent, the resonance absorption can explain best the experimental observation.

The qualitative simulation of the chirp effect was carried out by evaluating the multi-photon and avalanche rates for ionization of liquid sample by the linearly polarized pulse at right angle incidence. The ionisation potential of the target was taken $J = 8$ eV, which is an estimate considering the first orbital excitation of water molecules at 6.5 eV augmented by the quiver

#96969 - $15.00 USD Received 4 Jun 2008; revised 17 Jul 2008; accepted 29 Jul 2008; published 6 Aug 2008

energy ~ 1.5 in the case of fs-pulses as required by conservation laws [23].

The spectrally broad X-rays continuum is emitted from high temperature regions of plasma on the surface of target or departing overheated clusters via bremsstrahlung and the characteristic elemental transition are superimposed on the continuum [24]. Hence, the emission of X-rays is determined by the electron density and temperature. The modeling of temporal evolution of electron-ion density was made taking into account chirp of the femtosecond pulses. The electric field of a Gaussian pulse was taken in the form: $E(t) = E_0 e^{-2\ln 2\left(\frac{t}{\tau_p}\right)^2}\cos(\omega t + \beta t^2)$, where ω is the light's cyclic frequency, t is the time, τ_p is the pulse duration at a full-width at half maximum (FWHM), β [1/fs^2], is the chirp, and $E_0 = \sqrt{\frac{2I_0}{c\varepsilon_0 n}}$ is the electric field amplitude expressed via irradiance amplitude, I_0, light velocity, c, vacuum permittivity, ε_0, and refractive index, n ($n = 1$ for setting the focal spot from air onto surface of a water jet).

Evolution of the electron-ion generation rate during the pulse is modeled by simultaneously occurring multi-photon and avalanche (impact) ionization which have the probabilities $w_{mpi}(\omega_{ins}(t))$ and $w_{imp}(\omega_{ins}(t))$, respectively; here $\omega_{ins}(t) = \omega + 2\beta t$ is the instantaneous cyclic frequency of laser pulse in presence of the linear chirp. The positive chirp, $\beta > 0$, corresponds to the pulse where the frequency increases towards the pulse end and vice versa. Below a ~ 1 PW/cm^2 irradiance the contribution of a tunneling mechanism in a free electron generation is small, since the tunneling becomes dominant only when Keldysh parameter, $\gamma = \sqrt{2m_e J}\omega/(eE_0) << 1$ [19], here m_e and e are the mass and charge of electron, respectively. Hence, the $\sim$PW/cm^2 irradiance is required for tunneling to overcome the avalanche in multi-photon breakdown (the consideration given above is valid for the multi-photon process when $J/(\hbar\omega) \sim n_{ph} >> 1$ [19, 25]).

Temporal evolution of the electron density was calculated as in the case of breakdown of dielectrics [26]:

$$n_e(\omega_{ins}(t)) = \left(n_{e0} + \frac{n_a w_{mpi}}{w_{imp}}[1 - e^{-w_{imp}t}]\right) e^{w_{imp}t}, \tag{2}$$

where n_{e0} is the initial free electron density, which is $\sim 10^{12}$ cm^{-3} in dielectrics. The ionization probabilities depends on the instantaneous irradiance and frequency. The probabilities of impact and multi-photon ionization were taken in the form [27]: $w_{mpi} = \omega_{ins} n_{ph}^{3/2}\left(1.36\frac{\varepsilon_{osc}}{Jq}\right)^{n_{ph}}$, $w_{imp} = \frac{\varepsilon_{osc}}{Jq}\frac{2\omega_{ins}^2 \nu_{eff}}{\omega_{ins}^2 + \nu_{eff}^2}$, where $\varepsilon_{osc} = \frac{q^2 E_0^2}{4m\omega_{ins}^2}$ is the electron quiver energy in the electrical field of strength E_0, q and m are the electron charge and mass, respectively, n_{ph} is the number of photons necessary for ionization, $\nu_{eff} \simeq 6 \times 10^{14}$ Hz is an effective collision frequency in the breakdown plasma [26].

The results of simulation are shown in Fig. 4 for different chirp values. The positive and negative chirp resulted in faster electron generation rate than that of a transform-limited (chirp-free) pulse at irradiance $\sim$TW/cm^2. The positively chirped pulse with longer wavelength at the earlier times of light-solution interaction favors the avalanche over the multiphoton ionization since the electron quiver energy, $\varepsilon_{osc} \sim \lambda^2$ (see, dependencies of $w \propto \varepsilon_{osc}$). Indeed, the $w_{mpi} \simeq$ 42 THz and $w_{imp} \simeq 228$ THz at the irradiance of 30 TW/cm^2 with electron quiver energy of 1.64 eV. It should be noted that at much higher irradiance the multi-electron ionization should be considered with ionization potentials corresponding to the deeper electronic shells of ions. Hence, we limit discussion to a single ionization relevant to our experiments.

At the full breakdown conditions, the generation rate of electrons is faster on the earlier stages (at $t/\tau_p < 1$ in Fig. 4) for a positively chirped pulse. However, the largest electron density is predicted for the negatively chirped pulses when the multi-photon ionization efficiently contributes to generation of seeding electrons while the avalanche ($w_{imp} > w_{mpi}$ at the irradiance $\leq$50 TW/cm^2;) creates high plasma density (Fig. 4). This qualitative explanation is corrobo-

#96969 - $15.00 USD Received 4 Jun 2008; revised 17 Jul 2008; accepted 29 Jul 2008; published 6 Aug 2008

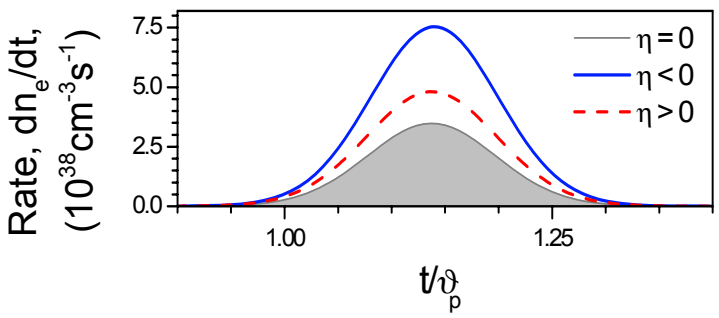

Fig. 4. (color online/final size) Evolution of ionisation rate dn_e/dt [cm^{-3}s^{-1}](calculated by eqn. 2) during the pulse of $\tau_p = 160$ fs duration at the positive and negative chirp $|\beta| = 6 \times 10^{-5}$ fs^{-2}, at which the pulse duration is 255 fs (see, Fig. 2(b)). Material has ionization potential $J = 8$ eV and the irradiance was $I = 30$ TW/cm^2.

rated experimentally (see, Fig. 2). The electron generation dynamics is very sensitive to the actual irradiance and chirp parameters; the electron generation rate would change significantly at different irradiance, pulse duration, and chirp parameters. Since the experimentally observed X-ray emission dependencies (Fig. 2) can be qualitatively well explained by the presented model, the influence of suprathermal electrons can be considered not significant at our experimental conditions. The electrons of high energy can escape from the surface of target and they will not contribute to X-ray generation due to reduced collisions in surrounding atmosphere. Also, the absorption cross-section of hot electrons decreases with temperature. The temperature of the hard X-rays was approximately same for the negatively and positively chirped pulses of 240 fs as well as for the transform-limited 160 ps pulses of the same energy (as can be judged from comparable slopes in log-lin plot; see, Supplement material). Hence, the experimentally observed scaling of the X-ray intensity depends mostly on the electron-ion concentration. Indeed, the emitted power via bremsstrahlung can be estimated as [28]:

$$P_{br} \sim Z^2 n_e n_i \sqrt{T_e}\ [\mathrm{W/m^3}], \tag{3}$$

where Z is the ionization number, $n_{e,i}$ [m^{-3}] are the electron and ion densities, respectively, and T_e is the electron temperature in electronvolts. The experimental data (Fig. 2) and the spectra (see, Supplement) show that the enhancement of X-ray emission was mostly determined by the electron concentration rather than by their temperature. Hence, the electron generation analysis was adequate for description of the observed X-ray generation enhancement.

4. Conclusions

The tenfold enhanced hard X-ray emission was observed for $p-$polarization and for negatively chirped fs-pulses. The dominant mechanism of X-ray generation is via the resonant absorption. This conclusion was supported by the experimentally measured angular dependence of X-ray generation. This study of chirp and angular dependence on X-ray emission could be useful for practical designs of X-ray sources. Combination of space and frequency chirps with tailored multi-pulse exposure of optimized duration, intra-pulse separation, and nano-plasma enhancement effects [29] are expected to further increase efficiency of X-ray generation in fs-plasma.

#96969 - $15.00 USD Received 4 Jun 2008; revised 17 Jul 2008; accepted 29 Jul 2008; published 6 Aug 2008

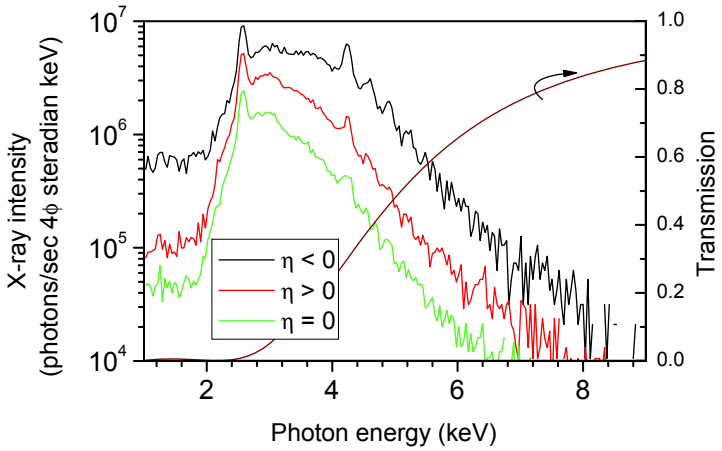

Fig. 5. (Supplement figure) Hard X-ray emission spectra for the negatively-chirped 240 fs, ($\beta < 0$) positively-chirped 240 fs ($\beta > 0$), and transform-limited 160 fs ($\beta = 0$) p-pol. pulses, respectively. Spectra are not corrected for the transmission in a 15-cm-long path in air; the transmission is shown on the right axis. The experimental conditions of X-ray generation are the same as those for Fig. 2 only the pulse energy was $E_p = 0.30$ mJ (at focus). The spectra were detected by the Si(Li) detector (Rontek, XFlash Detector Type 1100). The following lines of Cs and Cl can be recognized: the line at 2.55 keV (Cl $K\alpha$ at 2.62 keV), 4.26 keV (Cs $L\alpha$ at 4.28 keV), 4.60 keV (Cs $L\beta 1$ at 4.61 keV), and 4.89 keV (Cs $L\beta 2$ at 4.93 keV) according to the Ref. [X-ray data booklet, 2nd Edition, Center for X-ray Optics and Advanced Light Source Lawrence Berkeley National Laboratory, 2001].

Acknowledgments

This work was supported by KAKENHI (Grant-in-Aid for Scientific Research) on Priority Areas “Control of Molecules in Intense Laser Fields (No. 419, 14077202)” and “Strong Photon-Molecule Coupling Fields (No. 470, 20043002)” from the Ministry of Education, Culture, Sports, Science and Technology of Japan. S.J. is grateful for support provided by a Grant-in-Aid from the Ministry of Education, Science, Sports, and Culture of Japan No.19360322.

#96969 - $15.00 USD Received 4 Jun 2008; revised 17 Jul 2008; accepted 29 Jul 2008; published 6 Aug 2008